Spatially Inhomogeneous Metal-Insulator Transition in Doped Manganites

M. Fäth,[1] S. Freisem,[1] A. A. Menovsky,[1,2] Y. Tomioka,[3] J. Aarts,[1]* J. A. Mydosh[1]

Scanning tunneling spectroscopy was used to investigate single crystals and thin films of $La_{1-x}Ca_xMnO_3$ (with x of about 0.3), which exhibit colossal magnetoresistance. The different spectroscopic signatures of the insulating (paramagnetic) and metallic (ferromagnetic) phases enable their spatial extent to be imaged down to a lateral scale of the order of 10 nanometers. Above the bulk transition temperature T_c, the images show mostly insulating behavior. Below T_c, a phase separation is observed where inhomogeneous structures of metallic and more insulating areas coexist and are strongly field dependent in their size and structure. Insulating areas are found to persist far below T_c. These results suggest that the transition and the associated magnetoresistance behavior should be viewed as a percolation of metallic ferromagnetic domains.

The phenomenology of the colossal magnetoresistance (CMR) effect in doped rare-earth manganites of the type $R_{1-x}A_xMnO_3$ (R is a trivalent rare-earth ion and A is a divalent dopant) is described by interdependent transitions that take place in overlapping temperature ranges. For intermediate doping regimes, a metal-insulator transition (MIT) can occur, marked by a peak in the electrical resistivity ρ at a temperature T_p, from a high-temperature insulating phase ($d\rho/dT < 0$) to a low-temperature metallic phase ($d\rho/dT > 0$). This phase change is accompanied by a transition from a paramagnetic to a ferromagnetic phase, marked by the Curie temperature T_c at which spontaneous magnetization appears (see Fig. 1). Also in this temperature range, the local structure undergoes modifications involving rotations of the MnO_6 octahedra and changes of the Mn-Mn bond lengths. An example of this behavior is shown by the compound $La_{0.7}Ca_{0.3}MnO_3$, upon which our report is focused.

Although the theoretical understanding of the CMR phenomenon is still incomplete, double exchange (DE) (*1*), electron-phonon coupling (*2*), and orbital ordering effects (*3*) are commonly adopted as the main ingredients. The DE mechanism links the electronic to the magnetic transition and describes the hopping of electrons in e_g orbitals between neighboring Mn^{3+} and Mn^{4+} sites with strong on-site Hund's coupling by an O^{2-} ion. This charge transport is enhanced in the ferromagnetic state when the local Mn d-shell spins are parallel. In turn, the hopping electrons promote ferromagnetic order because they tend to preserve their spin direction. The random spin disorder in the crossover regime around T_c can be removed at least partially by applying a magnetic field. This shifts T_c and T_p to higher temperatures and causes CMR (negative) (Fig. 1). However, the DE mechanism alone is insufficient to correctly describe the high-temperature transport properties and to quantify the large resistance drop. At such temperatures, the insulator-like behavior results from electron localization caused by electron-lattice coupling, originating from local Jahn-Teller distortions at the Mn^{3+} site. These distortions also lift the degeneracy of the e_g orbitals, bringing orbital order (and disorder) into play.

Given these different interactions with very similar energy scales, the question of the ground state of the system is subtle. Evidence, accumulated from theory (*4*) and from experiment (see below), shows that spatial phase separation may occur between hole-rich [ferromagnetic metallic (FM)] and hole-poor (antiferromagnetic insulating) regions. This tendency should be least for doping in the middle of the FM regime (for example, $La_{0.7}Ca_{0.3}MnO_3$). Still, indications of charge inhomogeneities were reported at low temperatures from muon spin resonance (*5*), x-ray absorption (*6*), and optical experiments (*7*), whereas at high temperatures, polaron-like inhomogeneities were inferred from neutron scattering experiments (*8, 9*) and x-ray absorption (*10*). In all cases, the characteristic length of the localized charges, clusters, or polarons is of the order of a few lattice spacings, or 1 to 2 nm. All probes mentioned above yield average information from a macroscopic sample volume and allow only indirect conclusions to be drawn on the microscopic phase distribution. Here, we present real-space images of the local electronic properties of $La_{0.7}Ca_{0.3}MnO_3$ across the MIT, using scanning tunneling spectroscopy at temperatures between 4 and 300 K and in high magnetic fields of up to 9 T.

Samples of $La_{1-x}Ca_xMnO_3$ were investigated in single-crystalline bulk and thin-film form, which were characterized by electrical transport and magnetization measurements (as in Fig. 1), in addition to x-ray diffraction, electron probe microanalysis, and high-resolution electron microscopy (HREM). The two single crystals have Ca concentrations of $x = 0.25$ and $x = 0.3$. Epitaxial films of $La_{0.73}Ca_{0.27}MnO_3$ (*11*) with thicknesses between 10 and 100 nm were sputtered either directly on a $SrTiO_3$ substrate or on an epitaxial $YBa_2Cu_3O_y$ template layer to guarantee a low-resistive electrical contact to the sample volume close to the tip. The tunneling measurements were performed

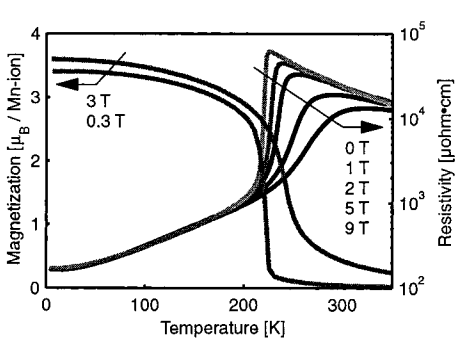

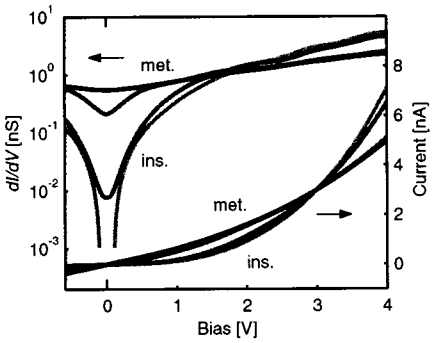

Fig. 1 (left). Temperature dependence of the Mn magnetic moment and electrical resistivity of a $La_{0.7}Ca_{0.3}MnO_3$ single crystal. The dc magnetization was measured in external fields of 0.3 and 3 T; the resistivity curves correspond to zero field measurements (top curve) and fields of 1, 2, 5, and 9 T (bottom curve). μ_B, Bohr magneton. **Fig. 2 (right).** Typical spectra for tunneling into (La,Ca)MnO_3 for the metallic (and semimetallic) ($T < T_c$) and semiconducting states ($T > T_c$), represented by nearly linear ("met.") and strongly curved ("ins.") *I-V* characteristics (bottom right) and by high ("met.") and low ("ins.") tunneling conductances, *dI/dV* (top left), respectively. Curves between the extremes indicate intermediate states in the gradual MIT.

[1]Kamerlingh Onnes Laboratory, Leiden University, Post Office Box 9504, 2300 RA Leiden, Netherlands. [2]Van der Waals–Zeeman Laboratory, University of Amsterdam, Valckenierstraat 67, 1018 XE Amsterdam, Netherlands. [3]Joint Research Center for Atom Technology, 1-1-4 Higashi, Tsukuba, Ibaraki 305-0046, Japan.

*To whom correspondence should be addressed. E-mail: aarts@phys.leidenuniv.nl

with a scanning tunneling microscope (STM) with $Pt_{0.9}Ir_{0.1}$ tips. For topographic scanning, the STM was operated at a relatively high bias voltage of typically 3 V in order to ensure sufficient current from bands above the semiconducting gap and to prevent tip-sample contact at low temperatures. Single crystals were cleaved immediately before the measurements, and thin films were measured instantly after deposition. In general, STM images show rather flat and smooth sample surfaces with variations in height of <20 nm on a lateral scale of several hundred nanometers. Local tunneling spectra were obtained by recording the tunneling current I as a function of bias voltage V at a fixed tip-sample separation of the order of 1 nm. We observed a temperature- and field-dependent gradual change of the tunneling characteristics that is expressed in the tunneling current (Fig. 2, bottom right) and the differential tunneling conductance dI/dV (Fig. 2, top left). Temperatures well above T_c yield typical semiconductor-like behavior, indicated by strongly curved I-V characteristics and vanishing conductance near the Fermi level at zero bias, which reflects the insulating energy gap. Well below T_c, the I-V characteristics are almost linear and display substantial zero-bias conductance, pointing to a finite density-of-states at the Fermi energy, as for a metal (or semimetal). To the best of our knowledge, this direct tunneling evidence for the MIT in the $(La,Ca)MnO_3$ system, which is in agreement with photoemission spectroscopy (*12*), has not been reported before. Previously, the MIT was linked to the appearance of distinct conductance peaks, despite a contradictory larger gap, in the bulk ferromagnetic state (*13*), which is not confirmed by our data. Good tunneling conditions during our measurements were verified by exponential tip-sample dependence of the current, topographic scanning without noticeable tip-sample contact, and independence of the normalized I-V spectra on the tunneling resistance. For clarity, we plotted only the positive bias part of the symmetrical spectra in Fig. 2.

Although the macroscopic MIT close to T_c is obvious in electrical resistivity, the situation is much different on a microscopic scale; that is, a metallic tunneling characteristic is not found at every location on the sample. In order to investigate this, we recorded scanning tunneling spectroscopic (STS) images simultaneously with topographic images by using a lock-in technique with a small (3%) modulation of the bias voltage, yielding the local differential conductance at a fixed bias of 3 V ($dI/dV|_{3\ V}$). The series of spectroscopic images from a thin-film sample (Fig. 3) is taken below but near T_c in magnetic fields between 0 and 9 T. Light colors correspond to high values of $dI/dV|_{3\ V}$ and, thus, to semiconducting tunneling behavior (see Fig. 2), whereas dark colors represent metallic characteristics. There are spatial variations of the local electronic properties on a submicrometer scale, demonstrating a coexistence of metallic and insulating, as well as intermediate, cloudlike regions. These "clouds" have typical sizes of tens of nanometers but can also form clusters of several hundred nanometers. The interpenetration of different phases appears self-similar down to an image size of the order of 20 nm. Such length scales are not compatible with a picture of homogeneously distributed small polarons, which are two orders of magnitude smaller, but it suggests localization effects due to spatial fluctuations of Coulomb and spin-dependent potentials as discussed, for example, by Coey *et al.* (*14*). Random potential fluctuations are conceivable even in single crystalline material due to, for example, site disorder of the Ca dopants or vacancies. By applying a magnetic field (Fig. 3), a considerable fraction of semiconducting (light) regions can be converted into metallic (dark) regions, resulting in metallic percolation paths throughout the sample. Similar to the bulk magnetization, this evolves fastest for modest fields (≤1 T) but continues up to 9 T and is largely reversible. Despite the fact that, with increasing magnetization, the system becomes increasingly metallic, some regions cannot be changed (even by fields as high as 9 T). Data very similar to those of Fig. 3 were obtained from a high-quality single crystal. The images show almost exclusively semiconducting behavior at temperatures far above the transition. On lowering the temperature, the system becomes more metallic on average as expected. However, there are always regions that remain insulating down to low temperatures far into the bulk FM state. The appearance of metallic and insulating regions is

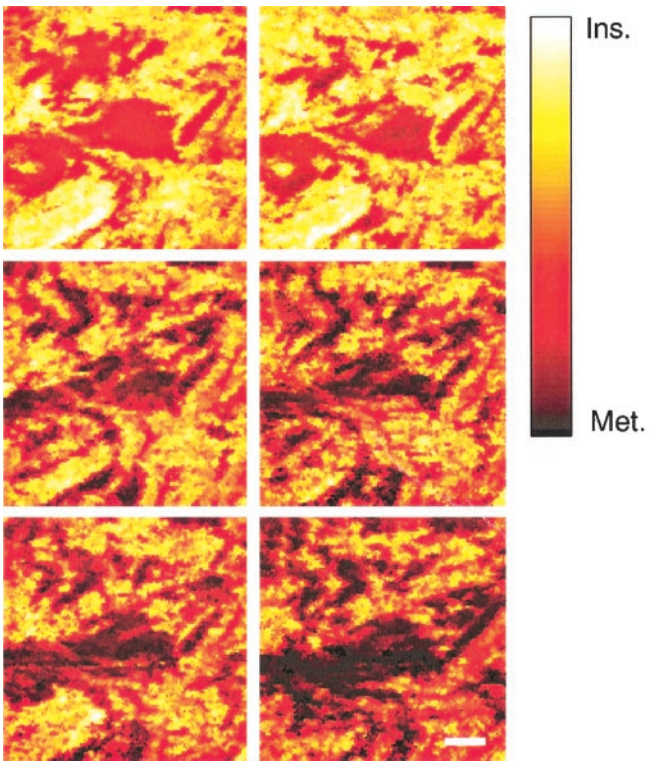

Fig. 3. Generic spectroscopic images (0.61 μm by 0.61 μm; scale bar, 100 nm) of the local electronic structure of $(La,Ca)MnO_3$ taken just below T_c in magnetic fields of 0, 0.3, 1, 3, 5, and 9 T (from left to right and top to bottom). Parts of the surface are insulating (light colors), whereas others are metallic (dark colors) or in an intermediate state. The color represents the slope of the local I-V spectrum at a bias of 3 V (see text and Fig. 2). The data were taken on a thin-film sample.

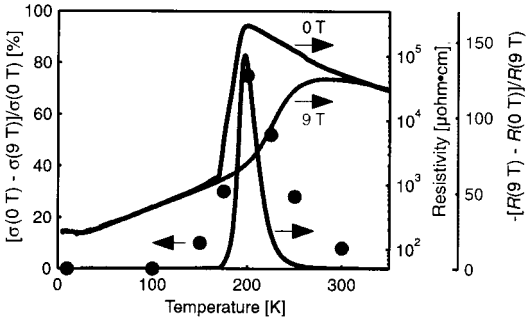

Fig. 4. Temperature dependence of resistivity in magnetic fields of 0 and 9 T and the corresponding magnetoresistance ratio of a $La_{0.75}Ca_{0.25}MnO_3$ single crystal (solid lines, right axes). The circles denote the relative change $[\sigma(0\ T) - \sigma(9\ T)]/\sigma\ (0\ T)$ to the metallic state of the image-averaged tunneling conductance ($\sigma = \overline{dI/cV}|_{3\ V}$) (Fig. 3) induced by a magnetic field of 9 T.

generally not related to the surface topography. Figure 4 shows a comparison of the temperature dependence of the CMR ratio $[R(0\ \mathrm{T}) - R(9\ \mathrm{T})]/R(9\ \mathrm{T})$, where R is the sample resistance, with the relative change in image brightness as determined from STS images similar to Fig. 3 in 0 and 9 T. There is excellent agreement between the temperature-dependent field sensitivity of our STS data and the magnetoresistive properties. This makes us confident that the tunneling measurements at the sample surface are representative for the bulk behavior and that the spectroscopic images can be regarded as two-dimensional cross sections of the three-dimensional sample volume.

The observations of the MIT and its spatial variations in the tunneling spectra are qualitatively the same for the various types of samples investigated. The cloudlike patterns signify static electronic inhomogeneities, which imply the existence of regions with different Mn oxidation states, meaning hole concentration. However, the phase separation is not as clear as in the case of $La_{0.5}Ca_{0.5}MnO_3$, where microdomains of a charge-ordered phase can be observed (*15*). Here, the phases do not appear to be fully metallic nor fully insulating, which might be a precursor to full separation. The origin of the observed phase separation is not yet clear, especially because at our doping concentration a homogeneous low-temperature state might be expected, with a dynamic rather than a static tendency for separation (*4*). It seems likely that structural disorder destroys the fragile balance in the system, which would help to explain the large length scales. Variations in the oxygen content are one possibility. Twinning is another; in both crystals, strong twinning on length scales of <100 nm was clearly observed by HREM (*16*). Such subtle disorder effects are unavoidable, even in state-of-the-art material; they should be taken into account in the interpretation of all current experiments and, in that sense, are an intrinsic part of the physics of the manganites. In this specific framework, our STS results force us to view the CMR as a magnetization-dependent phase separation that percolates, thereby generating a MIT.

References and Notes

1. C. Zener, *Phys. Rev.* **82**, 403 (1951).
2. A. J. Millis, *Nature* **392**, 147 (1998).
3. R. Maezono, S. Ishihara, N. Nagaosa, *Phys.Rev. B* **58**, 11583 (1998).
4. A. Moreo, S. Yunoki, E. Dagotto, *Science* **283**, 2034 (1999), and references therein.
5. R. H. Heffner *et al.*, *Phys. Rev. Lett.* **77**, 1869 (1996).
6. C. H. Booth *et al.*, *Phys. Rev. B* **57**, 10440 (1998).
7. S. Yoon *et al.*, *ibid.* **58**, 2795 (1998); H. L. Liu *et al.*, *ibid.*, p. R10115.
8. J. W. Lynn *et al.*, *Phys. Rev. Lett.* **76**, 4046 (1996).
9. J. M. De Teresa *et al.*, *Nature* **386**, 256 (1997).
10. A. Lanzara *et al.*, *Phys. Rev. Lett.* **81**, 878 (1998).
11. S. Freisem *et al.*, *J. Magn. Magn. Mater.* **165**, 380 (1997); J. Aarts *et al.*, *Appl. Phys. Lett.* **72**, 2975 (1998).
12. J.-H. Park *et al.*, *Phys. Rev. Lett.* **76**, 4215 (1996).
13. J. Y. T. Wei, N.-C. Yeh, R. P. Vasquez, *ibid.* **79**, 5150 (1997).
14. J. M. D. Coey, M. Viret, L. Ranno, *ibid.* **75**, 3910 (1995).
15. S. Mori, C. H. Chen, S.-W. Cheong, *ibid.* **81**, 3972 (1998).
16. H. W. Zandbergen, private communication.

17. We gratefully acknowledge discussions with J. Zaanen, D. Khomskii, A. Millis, and Y. Tokura. The work is supported in part by the Dutch Foundation for Fundamental Research of Matter (FOM) and by the New Energy and Industrial Technology Development Organization (NEDO) of Japan.

6 May 1999; accepted 19 July 1999

Stable Five- and Six-Coordinated Silicate Anions in Aqueous Solution

Stephen D. Kinrade,[1]* Jeffrey W. Del Nin,[1] Andrew S. Schach,[1] Todd A. Sloan,[1] Krista L. Wilson,[1] Christopher T. G. Knight[2]

Addition of aliphatic polyols to aqueous silicate solutions is shown to yield high concentrations of stable polyolate complexes containing five- or six-coordinated silicon. Coordinating polyols require at least four hydroxy groups, two of which must be in *threo* configuration, and coordinate to silicon via hydroxy oxygens at chain positions on either side of the *threo* pair. The remarkable ease by which these simple sugar-like molecules react to form hypervalent silicon complexes in aqueous solution supports a long-standing supposition that such species play a significant role in the biological uptake and transport of silicon and in mineral diagenesis.

The chemistry of silicon in the natural world is dominated by its affinity for oxygen, to which it is almost always tetrahedrally coordinated. Reports of naturally occurring pentaoxo- and hexaoxosilicon centers are very rare. In silicate minerals, five-coordinate centers are completely unknown, whereas six-coordinated silicon only occurs in high-pressure phases such as stishovite (*1*). In synthetic crystalline materials (including zeolite molecular sieves), only tetrahedral Si sites have been reported in cases where all coordinating atoms are oxygen. Silicate glasses are unique, however, in that they can contain silicon coordinated to four, five, or six oxygens, even when formed at atmospheric pressure, although the four-coordinate center remains by far the most common (*2*). A number of synthetic organosilicate complexes have been reported to contain hypervalent silicon (*3–9*). For example, mono- and dimeric pentacoordinate silicon glycolates form on dissolution of silica in ethylene glycol with an alkali-metal base (*3, 4*), and are implicated as intermediates in the nonaqueous synthesis of zeolites (*6*). The corresponding hexaalkoxysilicate species result when a group II metal oxide is used in place of the alkali-metal base (*5*). In aqueous solution, pentaoxosilicon is unknown and the hexaoxo-center is documented only for complexes in which silicon is chelated by catechol (yielding tris[1,2-benzenediolato]silicate) (*10*), 2-hydroxypyridine *N*-oxide (*11*), tropolone (*12*), or closely related analogs.

In an attempt to understand, on a molecular level, the formation of zeolites and microporous materials, we have studied the effects of alcohols and simple organic cations on the structure of aqueous silicate anions using ^{29}Si nuclear magnetic resonance (NMR) spectroscopy (*13*). We have observed in the course of this work that the addition of alkyl 1,2-diols to aqueous silicate solutions produces low concentrations of silicon-diolate complexes giving ^{29}Si NMR signals around -102 parts per million (ppm). These peaks closely correspond to those that Blohowiak *et al.* (*4*) and Herreros *et al.* (*6*) assign to five-coordinated silicon tris-glycolate complexes in H_2O-free ethylene glycol. However, the low concentrations of the complexes in aqueous solution prevent further structural refinement.

We report here that certain aliphatic polyhydroxy alcohols readily yield solutions containing high concentrations of stable hypervalent silicate anions. The silicon in these polyolate complexes can be in either five- or sixfold coordination by oxygen. The complexes are so stable that under favorable conditions they dominate the equilibrium, sometimes to the exclusion of the usual four-coordinate silicate species. In 11.7-T, ^{29}Si NMR spectra of a sodium silicate solution containing xylitol, three main peaks are noted

[1]Department of Chemistry, Lakehead University, 955 Oliver Road, Thunder Bay, Ontario, Canada P7B 5E1. [2]School of Chemical Sciences, University of Illinois at Urbana-Champaign, 600 South Mathews Avenue, Urbana, IL 61801, USA.

*To whom correspondence should be addressed. E-mail: Stephen.Kinrade@lakeheadu.ca